Single-Phase GaN-Based T-Type Totem-Pole Rectifier With Full-Range ZVS Control and Reactive Power Regulation

Jingjing Sun, *Student Member, IEEE*, Liyan Zhu, *Student Member, IEEE*, Ruiyang Qin, *Student Member, IEEE*, Daniel J. Costinett, *Senior Member, IEEE*, and Leon M. Tolbert, *Fellow, IEEE*

***Abstract*—This article proposes a high-efficiency single-phase GaN-based rectifier with reactive power transfer for use in front-end power supplies as an efficient alternative to centralized reactive power compensation. A full-range zero-voltage switching (ZVS) modulation for both unity power factor (PF) operation and nonunity PF operation is proposed for the GaN-based rectifier in critical conduction mode (CRM) operation. A frequency limitation method is also developed to limit the peak frequency during the ac current zero-crossing. Also, a GaN-based T-type totem-pole rectifier is proposed to overcome the control challenge in CRM during the ac voltage zero-crossing. Meanwhile, a digital-based control scheme is developed to implement ZVS operation and reactive power regulation. The proposed rectifier and ZVS control have the advantages of simple topology, high efficiency, straightforward control implementation, and capability of flexible reactive power regulation. A 1.6-kVA prototype of the GaN-based CRM T-type totem-pole rectifier is built and demonstrated with full-range ZVS operation, 98.9% full-load efficiency, and flexible reactive power regulation with smooth dynamic response.**

***Index Terms*—Critical conduction mode (CRM), gallium nitride (GaN), reactive power compensation, rectifier, soft switching, zero-voltage switching (ZVS).**

I. Introduction

REACTIVE power compensation is important for improving the grid power quality to achieve a high power transfer efficiency and maintain voltage stability [1], [2], [3]. Traditionally, centralized power compensators, such as static volt-ampere reactive (VAR) compensator and static synchronous compensator, are used for power quality management [4], [5]. Although providing flexible power compensation, conventional centralized power compensators are bulky, expensive, and exhibit large power loss [6], [7]. Also, with an increasing penetration of renewable energy and power electronics devices, the grid power quality is significantly impacted and may suffer from large voltage fluctuations that are difficult to deal with using traditional power compensators [8], [9], [10], [11].

On the other hand, grid support with load participation is a cost-effective approach to manage and control the power grid [12]. Critical loads, such as data centers and telecommunication power supplies, can also provide fast and flexible reactive power compensation with the front-end rectifiers in addition to active power transfer [13], [14]. Research efforts have been made on using single-phase grid-connected converters for reactive power compensation [13], [14], [15], [16], [17], [18], [19], [20]. In [17] and [18], reactive power regulation was integrated in diode-based rectifiers. However, due to the characteristic of diode unidirectional current flow, an uncontrollable region appears whenever the polarities of current and voltage become opposite, leading to severe input current distortion and limited capability of reactive power compensation.

Active front-end rectifiers, such as metal oxide semiconductor field effect transistor (MOSFET)-based full-bridge pulse width modulation (PWM) converter and totem-pole power factor correction (PFC) rectifier, allow bidirectional power flow and are able to achieve reactive power operation with wide power factor (PF) range and low input current distortion [13], [14], [19], [20]. Typically, to control the reactive power, the instantaneous reactive power Q is calculated based on a power estimator where the single-phase ac voltage and current are sensed and decoupled into dq rotating frame for Q calculation [14], [20]. In [13], a control scheme of regulating both the active power and reactive power was developed in a full-bridge PWM rectifier for telecommunication application. The outer power loops regulate P and Q and generate current references in d- and q-axis. The inner current loop determines the duty cycle, which is used in a PWM modulator for controlling the rectifier. In [19], reactive power control was applied in an on-board bidirectional electric vehicle (EV) charger, which was demonstrated to provide reactive power for grid support and active power for battery charging/discharging simultaneously. Nevertheless, existing work on the single-phase converter with reactive power operation concentrates on Si-based hard switching PWM converters, which have low efficiency and low power density.

Manuscript received 15 May 2022; revised 23 July 2022 and 14 September 2022; accepted 10 October 2022. Date of publication 20 October 2022; date of current version 18 November 2022. This work was supported in part by Engineering Research Center Shared Facilities supported by the Engineering Research Center Program of the National Science Foundation and DOE under NSF under Grant EEC-1041877 and in part by CURENT Industry Partnership Program. Recommended for publication by Associate Editor X. Ruan.

The authors are with the Min H. Kao Department of Electrical Engineering and Computer Science, University of Tennessee, Knoxville, TN 37996-2250 USA (e-mail: jsun30@vols.utk.edu; lzhu21@vols.utk.edu; rqin1@vols.utk.edu; daniel.costinett@utk.edu; tolbert@utk.edu).

Color versions of one or more figures in this article are available at https://doi.org/10.1109/TPEL.2022.3215969.

Digital Object Identifier 10.1109/TPEL.2022.3215969

Recently, gallium nitride (GaN)-based totem-pole PFC rectifier has become popular for use in front-end power supplies, which is advantageous in simple topology, capability of achieving zero-voltage switching (ZVS), and the superior properties of GaN device, including low on resistance, high switching speed, and zero reverse recovery loss [21], [22], [23]. By adopting critical conduction mode (CRM) operation and ZVS control, a GaN-based totem-pole PFC rectifier can achieve soft switching over the whole line cycle and has been demonstrated with 99% peak efficiency [24], [25], [26]. Since switching loss is minimized, the converter's switching frequency can be pushed to hundreds of kHz or even MHz, and high-power density is achieved [24], [27], [28]. Based on the single-phase totem-pole PFC, topologies, such as interleaved totem-pole PFC [24], [29] and multilevel totem-pole PFC [30], [31], have also been developed to help reduce current ripple, decrease device voltage stress, and mitigate noise level.

If the high-efficiency, high-density GaN-based rectifier is able to transfer reactive power for grid support, the power loss for reactive power compensation can be significantly reduced. However, few research works study the reactive power operation of the single-phase GaN-based converter with soft switching. In [32], reactive power operation of a CRM totem-pole inverter with ZVS control was simulated. However, a method for overcoming the implementation challenge during ac line zero-crossing is not provided, and no further detailed analysis and hardware design are provided.

With a focus on the single-phase GaN-based CRM rectifier, this article studies the topology, ZVS modulation, and control for achieving reactive power regulation. A GaN-based CRM T-type totem-pole rectifier is proposed, which is advantageous in transferring both active and reactive powers, achieving full-range ZVS control for both unity PF operation and nonunity PF operation, overcoming the control challenge during ac voltage zero-crossing while maintaining the properties of high efficiency, simple topology, and control implementation. A 1.6-kVA GaN-based T-type totem-pole rectifier prototype is designed and demonstrated with full-range ZVS operation in CRM, 98.9% full-load efficiency, and flexible reactive power transfer from leading 0.79 to lagging 0.87 PF.

The rest of this article is organized as follows. Section II introduces the GaN-based T-type totem-pole rectifier. Section III illustrates the full-range ZVS modulation with peak frequency limitation. Section IV presents the control strategy for ZVS operation and reactive power regulation. Section V shows the experimental verification. Finally, Section VI concludes this article.

II. Rectifier Topology

A. CRM Totem-Pole Rectifier

The GaN-based CRM totem-pole PFC rectifier achieves high efficiency with ZVS control. The topology is regarded as a promising candidate for front-end rectifiers in applications of consumer electronics, data centers, and EVs [26], [33], [34]. As shown in Fig. 1, S_1 and S_2 are the GaN transistors operating at fast switching frequency and S_3 and S_4 are the Si MOSFETs working at ac line frequency. In unipolar modulation, S_3 and S_4 need to be switched at the v_{in} zero-crossing points. During

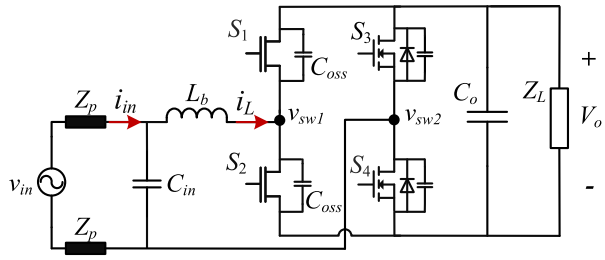

Fig. 1. GaN-based totem-pole PFC rectifier.

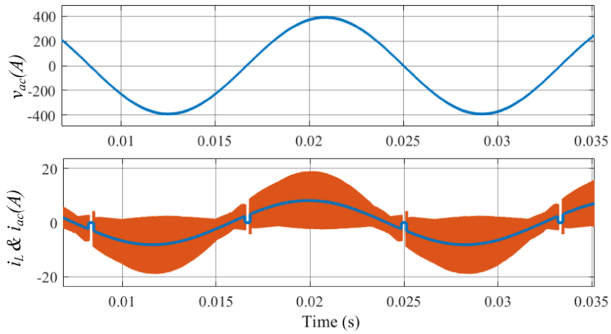

Fig. 2. Simulation waveforms of the CRM totem-pole rectifier at 0.94 leading PF with 200-μs blanking time during the ac voltage zero-crossing when $v_{\text{in}} = 277\,\text{V}_{\text{ac}}, V_o = 480\,\text{V}_{\text{dc}}, P = 1.5\,\text{kW},$ and $Q = -500\,\text{VAr}$.

the negative half-line cycle, S_3 is ON, S_4 is OFF, S_1 is the active switch (AS), and S_2 is the synchronous rectification switch (SS). During the positive half-line cycle, S_4 is ON, S_3 is OFF, S_2 is AS, and S_1 is SS. To achieve ZVS turn-ON of GaN devices, the rectifier operates in CRM where i_L reaches to zero in each switching cycle and the inductor resonates with GaN devices' output capacitances during the dead time. In practical implementation, ac voltage zero-crossing distortion is a common issue for the GaN-based totem-pole PFC rectifier [35], [36], [37]. In unipolar modulation, the voltage applied on the inductor is v_{in} when AS is on, and v_{in} is near zero in the vicinity of the zero-crossing points, leading to a long conduction time and low switching frequency in CRM operation [32]. Also, because of the inaccurate v_{in} zero-crossing detection, sensing delay, switching noise, and different commutation time between Si MOSFET and GaN deivice, the Si MOSFET switching moment is not perfectly synchronized with the v_{in} zero-crossing point. This makes the inductor current out of control during v_{in} zero-crossing region, resulting in large current spike and unstable operation. To overcome this ac voltage zero-crossing issue, typically, a blanking time (typically 200 μs) with specified device switching pattern is adopted [25], [37], [38], [39].

Nevertheless, the blanking-time approach is not applicable in the case with reactive power operation. Fig. 2 shows the simulation results of the CRM totem-pole rectifier with leading PF, and a blanking time is implemented during the ac voltage zero-crossing. Since the ac current is not zero at the ac voltage zero-crossing, during the blanking time, the inductor current suddenly drops to zero and the ac current abruptly changes to be equal to the current flowing through the input capacitor, leading to observable input current distortion. Fig. 3 shows

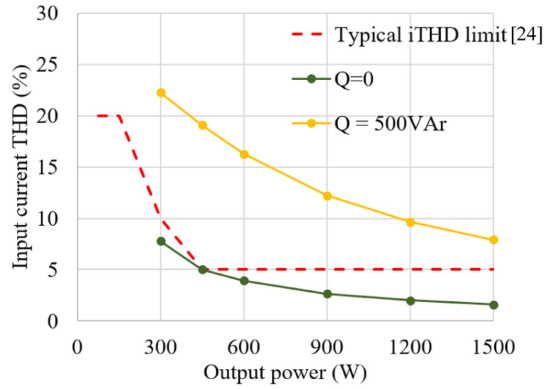

Fig. 3. Input current THD of the CRM totem-pole rectifier at various power levels with 200-μs blanking time when $V_{\text{in}} = 277\,\text{V}_{\text{ac}}$ and $V_o = 480\,\text{V}_{\text{dc}}$.

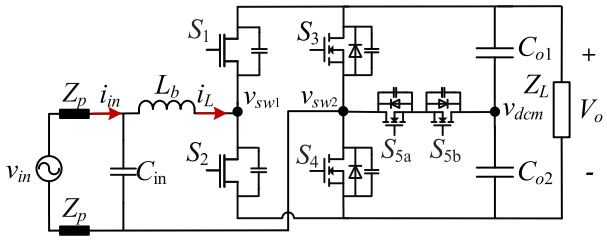

Fig. 4. Proposed GaN-based T-type totem-pole rectifier.

the predicted input current total harmonic distortion (THD) of the CRM totem-pole rectifier with blanking time. The current THD becomes much worse with reactive power. Therefore, an alternative solution is required to overcome the ac voltage zero-crossing issue of the GaN-based CRM totem-pole rectifier with reactive power.

B. Proposed CRM T-Type Totem-Pole Rectifier

To overcome the ac voltage zero-crossing challenge, a modified totem-pole rectifier is proposed, as shown in Fig. 4. A bidirectional switch S_5, which is composed of two antiseries connected Si MOSFETs S_{5a} and S_{5b}, is inserted between the Si phase leg and the dc capacitor. Since a T-type structure is constructed, the topology is called T-type totem-pole rectifier. The two additional active devices (i.e., S_{5a} and S_{5b}) operate at ac line frequency and only conduct for a short time during the ac voltage zero-crossing. Hence, only slight power loss is added and the control of S_5 is simple.

The rectifier has two operation modes: totem-pole mode and T-type mode. Fig. 5 illustrates the device switching pattern of the T-type totem-pole rectifier. An intermediate boundary voltage V_{boun} is defined to distinguish the two operation modes. When $|V_{\text{in}}| > V_{\text{boun}}$, the rectifier operates in the normal totem-pole mode with unipolar modulation. Bidirectional switch S_5 is OFF, S_3 conducts during the negative half cycle and S_4 conducts during the positive half cycle. S_1 and S_2 switch at high frequency with the same ZVS modulation as the unity-PF CRM totem-pole PFC [22]. When $|V_{\text{in}}| \le V_{\text{boun}}$, the rectifier operates in T-type mode with S_5 ON and S_3 and S_4 OFF. S_1 and S_2 are still high-frequency devices. Since T-type mode is only adopted during the voltage zero-crossing region, V_{boun} is

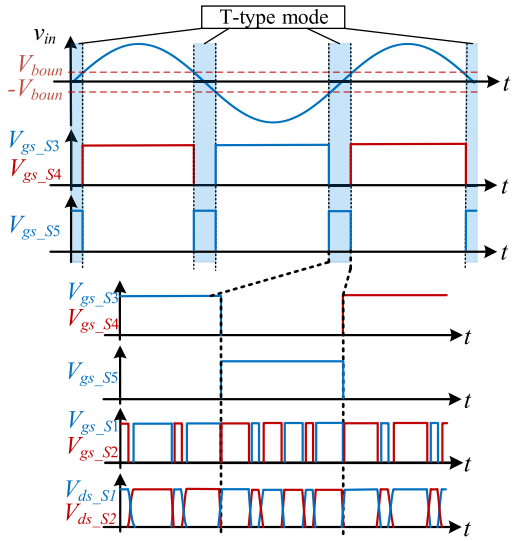

Fig. 5. Device switching sequence of the T-type totem-pole rectifier.

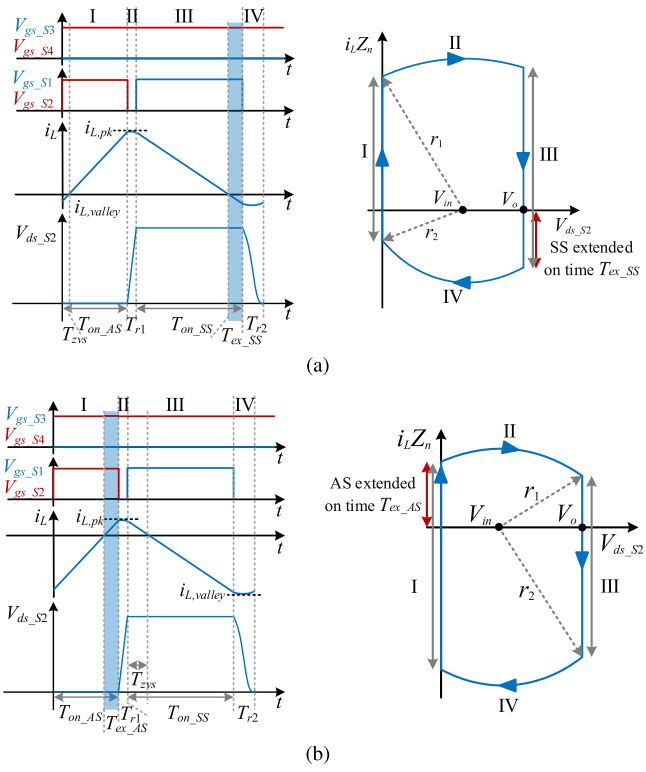

Fig. 6. ZVS waveforms and state-plane trajectory during totem-pole mode when (a) $V_{\text{in}} > 0$, $I_{\text{in}} > 0$; and (b) $V_{\text{in}} > 0$, $I_{\text{in}} < 0$.

typically small, e.g., $V_{\text{boun}} < 0.25V_o$. Hence, during the T-type mode, the boost inductor is charged with $v_L = V_{\text{in}} + 0.5V_o > 0$ when S_2 conducts and discharged with $v_L = V_{\text{in}} - 0.5V_o < 0$ when S_1 is ON. In this way, the inductor voltage is dominated by the output voltage and is always under control. Also, because of the T-type mode operation, switching moments of Si MOSFETs (i.e., $S_3, S_4,$ and S_5) do not need to be synchronized with the ac voltage zero-crossing point. Therefore, even with nonideal condition, such as sensing delay and switching noise, the control will remain stable without current distortion during the voltage zero-crossing.

III. Full-Range ZVS Modulation in CRM

To analyze ZVS operation principle with reactive power transfer, the rectifier waveforms and state-plane trajectories within one switching cycle are illustrated. Due to the symmetric characteristic, the following discussion will only consider the positive half-line cycle of the input voltage, and assumes that the input voltage remains constant within one switching cycle. For the state-plane trajectories, the characteristic impedance Z_n is defined as $Z_n^2 = \frac{L_b}{(2C_{oss})}$, where C_{oss} is the equivalent drain-to-source capacitance of S_1 and S_2, assuming $C_{oss,S1} = C_{oss,S2} = C_{oss}$.

A. Review of Basic ZVS Modulation At Unity PF

The full-line cycle ZVS modulation of the CRM totem-pole PFC rectifier has been illustrated in the previous research [22], [25]. In unipolar modulation, the inductor current is charged with V_{in} when AS S_2 conducts and discharged with $(V_{\text{in}} - V_o)$ when synchronous rectification switch (SS) S_1 is ON. As shown in Fig. 6(a), S_1 achieves ZVS turn-ON naturally since $i_{L,pk}$ discharges $C_{oss,S1}$ during the dead time T_{r1} before S_1 turns ON. However, S_2 can only achieve natural ZVS turn-ON when $V_{\text{in}} \le 0.5V_o$. When $V_{\text{in}} > 0.5V_o$, $i_{L,\text{valley}}$ is not enough to fully discharge $C_{oss,S2}$ before S_2 turns ON, leading to valley switching [24]. To also realize ZVS when $V_{\text{in}} > 0.5V_o$, the conduction time of S_1, $T_{\text{on\_SS}}$, is extended by $T_{\text{ex\_SS}}$ to have a lower $i_{L,\text{valley}}$ so that V_{ds_S2} is able to resonate to zero before S_2 turns ON.

In order to ensure ZVS in each switching cycle, a ZVS margin constraint k is defined as

$$k = \frac{r_1}{V_{\text{in}}} = \begin{cases} \frac{V_o - V_{\text{in}}}{V_{\text{in}}}, & V_{\text{in}} \le V_{\text{bound,zvs}} \\ k_0, & V_{\text{in}} > V_{\text{bound,zvs}} \end{cases} \quad (1)$$

where $k_0 > 1$ is the selected ZVS margin and $V_{\text{bound,zvs}} = \frac{V_o}{(k_0+1)}$ is the boundary input voltage between natural ZVS region and non-natural ZVS region. Based on the state trajectory [see Fig. 6(a)], the extended conduction time is

$$T_{\text{ex\_SS}} = \frac{\sqrt{(k^2-1)V_{\text{in}}^2 - V_o^2 + 2V_oV_{\text{in}}}}{w_r(V_o - V_{\text{in}})} \quad (2)$$

where $w_r^2 = \frac{1}{(2C_{oss}L_b)}$ is the resonant angle frequency. When $V_{\text{in}} \le V_{\text{bound,zvs}}$, $T_{\text{ex\_SS}} = 0$; when $V_{\text{in}} > V_{\text{bound,zvs}}$, $T_{\text{ex\_SS}} > 0$. More detailed illustration on the ZVS modulation of the CRM totem-pole PFC rectifier is presented in [22] and [25].

B. Proposed ZVS Modulation During Totem-Pole Mode

During the totem-pole mode with S_5 OFF, when $V_{\text{in}} > 0, I_{\text{in}} > 0$ [see Fig. 6(a)], the rectifier operates in the same way as the conventional CRM totem-pole PFC rectifier. S_1 turns ON naturally with ZVS, and S_1 conduction $T_{\text{on\_SS}}$ is extended by $T_{\text{ex\_SS}}$ to help achieve S_2 ZVS turn-ON when $V_{\text{in}} > V_{\text{bound,zvs}}$.

When $V_{\text{in}} > 0, I_{\text{in}} < 0$ [see Fig. 6(b)], S_2 achieves ZVS turn-ON passively since $|i_{L,\text{valley}}|$ is large enough to discharge $C_{oss,S2}$. However, S_1 only realizes valley switching when $V_{\text{in}} < 0.5V_o$. To achieve S_1 ZVS turn-ON, the conduction time of S_2, $T_{\text{on\_AS}}$, is extended by $T_{\text{ex\_AS}}$ for a larger $|i_{L,pk}|$.

Based on the same modeling principle, the generalized coefficient k is extended to represent ZVS achievement for both unity PF operation and nonunity PF operation. Table I gives the key modeling parameters for ZVS modulation in the four quadrants of V_{in} and I_{in}. k_{lim} is the coefficient for peak frequency limitation, which is illustrated in Section III-D.

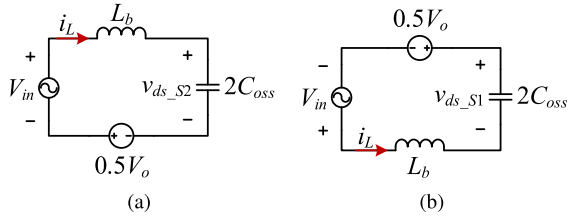

Fig. 7. Resonant equivalent circuits of the T-type totem-pole rectifier during the T-type mode when (a) $V_{\text{boun}} \ge V_{\text{in}} > 0$; and (b) $-V_{\text{boun}} \le V_{\text{in}} < 0$.

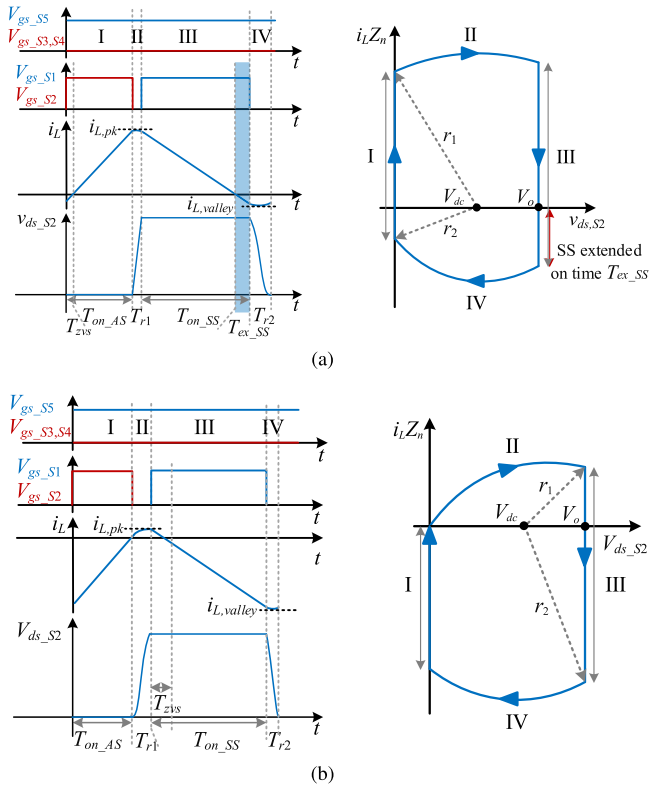

Fig. 8. ZVS waveforms and state-plane trajectory during T-type mode when (a) $V_{\text{in}} > 0, I_{\text{in}} > 0$; and (b) $V_{\text{in}} > 0, I_{\text{in}} < 0$.

C. Proposed ZVS Modulation During T-Type Mode

To maintain the full-range ZVS operation, ZVS modulation during the T-type mode is also proposed. Fig. 7 shows the equivalent circuit during the resonance in the T-type mode, where the voltage across the dc capacitor is represented by a constant voltage source at $0.5V_o$ and $2C_{oss}$ is the equivalent output capacitance of S_1 and S_2. When $V_{\text{boun}} \ge V_{\text{in}} > 0$, S_2 is the AS, and the dc voltage applied on $2C_{oss}$ is $V_{\text{dc}} = (V_{\text{in}} + 0.5V_o) > 0.5V_o$. When $-V_{\text{boun}} \le V_{\text{in}} < 0$, S_1 is the AS, and the dc voltage across $2C_{oss}$ is $V_{\text{dc}} = (-V_{\text{in}} + 0.5V_o) > 0.5V_o$. Therefore, the dc solution of the state-plane for ZVS analysis is $(|V_{\text{in}}| + 0.5V_o,\ 0)$.

Fig. 8 shows the switching waveforms and state-plane trajectories of the T-type totem-pole rectifier during the T-type mode with positive v_{in}. When $V_{\text{in}} > 0, I_{\text{in}} > 0$ [see Fig. 8(a)], S_1 realizes ZVS naturally, but S_2 can only achieve valley

TABLE I
ZVS OPERATION PRINCIPLE OF THE GAN-BASED CRM T-TYPE TOTEM-POLE RECTIFIER DURING TOTEM-POLE MODE

Positive half-line cycle of the input voltage		
Parameter	$V_{\text{in}} > 0, I_{\text{in}} > 0$	$V_{\text{in}} > 0, I_{\text{in}} < 0$
AS	S_2	S_2
Synchronous switch (SS)	S_1	S_1
AS natural ZVS region	$V_{\text{in}} \le V_{\text{bound,zvs}}, \quad V_{\text{bound,zvs}} = \frac{V_o}{k_0+1}$	all range
SS natural ZVS region	all range	$V_{\text{in}} \ge V_{\text{bound,zvs}}, \quad V_{\text{bound,zvs}} = \frac{k_0 V_o}{k_0+1}$
ZVS constraint	$k = \begin{cases} \max\{k_{\text{lim}}, \frac{V_o - V_{\text{in}}}{V_{\text{in}}}\}, V_{\text{in}} \le V_{\text{bound,zvs}} \\ \max\{k_{\text{lim}}, k_0\}, \qquad V_{\text{in}} > V_{\text{bound}} \end{cases}$	$k = \begin{cases} \max\{k_{\text{lim}}, \frac{V_{\text{in}}}{V_o - V_{\text{in}}}\}, V_{\text{in}} \ge V_{\text{bound,zvs}} \\ \max\{k_{\text{lim}}, k_0\}, \qquad V_{\text{in}} < V_{\text{bound}} \end{cases}$
Extended ON time	$T_{\text{ex\_SS}} = \frac{\sqrt{(k^2-1)V_{\text{in}}^2 - V_o^2 + 2V_o V_{\text{in}}}}{w_r(V_o - V_{\text{in}})}$	$T_{\text{ex\_AS}} = \frac{\sqrt{(k^2-1)V_{\text{in}}^2 + V_o^2 - 2V_o V_{\text{in}}}}{w_r V_{\text{in}}}$
Negative half-line cycle of the input voltage		
Parameter	$V_{\text{in}} < 0, I_{\text{in}} > 0$	$V_{\text{in}} < 0, I_{\text{in}} < 0$
AS	S_1	S_1
Synchronous switch (SS)	S_2	S_2
AS natural ZVS region	all range	$-V_{\text{in}} \le V_{\text{bound,zvs}}, \quad V_{\text{bound,zvs}} = \frac{V_o}{k_0+1}$
SS natural ZVS region	$-V_{\text{in}} \ge V_{\text{bound,zvs}}, \quad V_{\text{bound,zvs}} = \frac{k_0 V_o}{k_0+1}$	all range
ZVS constraint	$k = \begin{cases} \max\{k_{\text{lim}}, \frac{-V_{\text{in}}}{V_o + V_{\text{in}}}\}, -V_{\text{in}} \ge V_{\text{bound,zvs}} \\ \max\{k_{\text{lim}}, k_0\}, \qquad -V_{\text{in}} < V_{\text{bound}} \end{cases}$	$k = \begin{cases} \max\{k_{\text{lim}}, \frac{V_{\text{in}} + V_o}{-V_{\text{in}}}\}, -V_{\text{in}} \le V_{\text{bound,zvs}} \\ \max\{k_{\text{lim}}, k_0\}, \qquad -V_{\text{in}} > V_{\text{bound}} \end{cases}$
Extended ON time	$T_{\text{ex\_SS}} = \frac{\sqrt{(k^2-1)V_{\text{in}}^2 + V_o^2 + 2V_o V_{\text{in}}}}{-w_r V_{\text{in}}}$	$T_{\text{ex\_AS}} = \frac{\sqrt{(k^2-1)V_{\text{in}}^2 - V_o^2 - 2V_o V_{\text{in}}}}{w_r(V_o + V_{\text{in}})}$

switching because $(|V_{\text{in}}| + 0.5V_o) \ge 0.5V_o$ and $|i_{L,\text{valley}}|$ is not large enough to discharge $C_{oss,S2}$. Therefore, ZVS extension is required by increasing the conduction time of S_1 to enlarge $|i_{L,\text{valley}}|$ and gain more inductor energy for the resonance. When $V_{\text{in}} > 0, I_{\text{in}} < 0$ [see Fig. 8(b)], both GaN devices can achieve ZVS turn-ON naturally and ZVS extension is not required. Considering the peak switching frequency limitation, ZVS operation principle during the T-type mode is given in Table II.

D. Proposed Peak Frequency Limitation

One issue of the CRM operation with reactive power transfer is the high-peak switching frequency at the ac current zero-crossing. This is because the zero-crossing points of i_{in} and v_{in} are no longer at the same moment with the phase shift. During the ac current zero-crossing, v_{in} is not zero, leading to very high switching frequency to maintain the CRM operation [see Fig. 9(a)]. Such high switching frequency would result in worse electromagnetic interference (EMI) noise as well as higher switching loss and gate drive loss.

A frequency limitation method is proposed to reduce the peak frequency by modifying the ZVS margin constraint k. To simplify the calculation of switching period t_{sw}, the inductor current is approximated as a triangular waveform with linear increase from $i_{L,\text{valley}}$ to $i_{L,pk}$ and linear decrease from $i_{L,pk}$ to $i_{L,\text{valley}}$. Thus, the switching period is expressed as

$$t_{\text{sw}} = \frac{1}{f_{\text{sw}}} \approx L_b \frac{i_{L,pk} - i_{L,\text{valley}}}{v_{L,\text{rise}}} + L_b \frac{i_{L,pk} - i_{L,\text{valley}}}{-v_{L,\text{fall}}} \tag{3}$$

where $v_{L,\text{rise}} > 0$ and $v_{L,\text{fall}} < 0$ are the voltages applied on the inductor during i_L rising and falling, respectively.

Assume $f_{s\max}$ is the allowable maximum switching frequency, f_s should be lower than $f_{s\max}$, that is,

$$t_{\text{sw}} \ge \frac{1}{f_{s\max}}. \tag{4}$$

Combining (3) and (4), the required inductor current ripple is

$$i_{L,pk} - i_{L,\text{valley}} \ge \frac{-v_{L,\text{rise}} v_{L,\text{fall}}}{L_b f_{s\max}(v_{L,\text{rise}} - v_{L,\text{fall}})}. \tag{5}$$

Since $i_{L,pk} + i_{L,\text{valley}} = 2i_{L,\text{ave}} \approx 2i_{\text{in}}$, together with (5), the inductor current limit is

$$i_{L,pk} \ge i_{\text{in}} + \frac{-v_{L,\text{rise}} v_{L,\text{fall}}}{2L_b f_{s\max}(v_{L,\text{rise}} - v_{L,\text{fall}})} \tag{6}$$

TABLE II
ZVS OPERATION PRINCIPLE OF THE GAN-BASED CRM T-TYPE TOTEM-POLE RECTIFIER DURING T-TYPE MODE

Positive half-line cycle of the input voltage		
Parameter	$V_{\text{boun}} \geq V_{\text{in}} > 0, I_{\text{in}} > 0$	$V_{\text{boun}} \geq V_{\text{in}} > 0, I_{\text{in}} < 0$
AS	S_2	S_2
Synchronous switch (SS)	S_1	S_1
AS natural ZVS region	no range	all range
SR natural ZVS region	all range	all range
Full-range ZVS constraint	$k = \max\{k_0, k_{\text{lim}}\}$	$k = \max\{1, k_{\text{lim}}\}$
Extended ON time	$T_{\text{ex\_SS}} = \frac{\sqrt{k^2(V_{\text{in}}+0.5V_o)^2-(0.5V_o-V_{\text{in}})^2}}{w_r(0.5V_o-V_{\text{in}})}$	$T_{\text{ex\_AS}} = 0$
Negative half-line cycle of the input voltage		
Parameter	$-V_{\text{boun}} \leq V_{\text{in}} < 0, I_{\text{in}} > 0$	$-V_{\text{boun}} \leq V_{\text{in}} < 0, I_{\text{in}} < 0$
AS	S_1	S_1
Synchronous switch (SS)	S_2	S_2
AS natural ZVS region	all range	no range
SR natural ZVS region	all range	all range
Full-range ZVS constraint	$k = \max\{1, k_{\text{lim}}\}$	$k = \max\{k_0, k_{\text{lim}}\}$
Extended ON time	$T_{\text{ex\_AS}} = 0$	$(T_{\text{ex\_SS}} = \frac{\sqrt{k^2(-V_{\text{in}}+0.5V_o)^2-(0.5V_o+V_{\text{in}})^2}}{w_r(0.5V_o+V_{\text{in}})}$

TABLE III
ZVS CONSTRAINT LIMITATION k_{LIM} FOR PEAK FREQUENCY LIMITATION OF THE CRM TOTEM-POLE RECTIFIER

Positive half-line cycle of the input voltage		
	$V_{\text{in}} > 0, I_{\text{in}} > 0$	$V_{\text{in}} > 0, I_{\text{in}} < 0$
k_{lim}	$(I_{\text{in}} + \frac{V_{L,\text{rise}}V_{L,\text{fall}}}{2L_b f_{s\max}(V_{L,\text{rise}}-V_{L,\text{fall}})})\frac{Z_n}{-V_{L,\text{rise}}}$	$(I_{\text{in}} - \frac{V_{L,\text{rise}}V_{L,\text{fall}}}{2L_b f_{s\max}(V_{L,\text{rise}}-V_{L,\text{fall}})})\frac{Z_n}{-V_{L,\text{fall}}}$
Negative half-line cycle of the input voltage		
	$V_{\text{in}} < 0, I_{\text{in}} > 0$	$V_{\text{in}} < 0, I_{\text{in}} < 0$
k_{lim}	$(I_{\text{in}} - \frac{V_{L,\text{rise}}V_{L,\text{fall}}}{2L_b f_{s\max}(V_{L,\text{rise}}-V_{L,\text{fall}})})\frac{Z_n}{-V_{L,\text{fall}}}$	$(I_{\text{in}} + \frac{V_{L,\text{rise}}V_{L,\text{fall}}}{2L_b f_{s\max}(V_{L,\text{rise}}-V_{L,\text{fall}})})\frac{Z_n}{-V_{L,\text{rise}}}$

or

$$i_{L,\text{valley}} \leq i_{\text{in}} - \frac{-v_{L,\text{rise}}v_{L,\text{fall}}}{2L_b f_{s\max}(v_{L,\text{rise}} - v_{L,\text{fall}})}. \quad (7)$$

When $i_{\text{in}} > 0$, $i_{L,\text{valley}} = \frac{-kv_{\text{rise}}}{Z_n}$. Inserting $i_{L,\text{valley}}$ into (7), the ZVS constraint k is

$$k \geq k_{\text{lim}} = \left(i_{\text{in}} + \frac{v_{L,\text{rise}}v_{L,\text{fall}}}{2L_b f_{s\max}(v_{L,\text{rise}} - v_{L,\text{fall}})}\right)\frac{Z_n}{-v_{L,\text{rise}}}. \quad (8)$$

Similarly, when $i_{\text{in}} < 0$, $i_{L,pk} = \frac{-kv_{\text{fall}}}{Z_n}$. Inserting $i_{L,pk}$ into (6), the ZVS constraint k is

$$k \geq k_{\text{lim}} = \left(i_{\text{in}} - \frac{v_{L,\text{rise}}v_{L,\text{fall}}}{2L_b f_{s\max}(v_{L,\text{rise}} - v_{L,\text{fall}})}\right)\frac{Z_n}{-v_{L,\text{fall}}}. \quad (9)$$

Similar analysis is also applied for the negative half cycle, and Table III gives the required k for peak frequency limitation in the four quadrants of V_{in} and I_{in}. In the control implementation, accurate calculation of k is important, which is enabled by near-constant impedance parameters (i.e., L_b and Z_n) and accurate voltage sensing.

Fig. 9(b) shows the analytical waveforms of the CRM T-type totem-pole rectifier at 0.79 leading PF with peak frequency

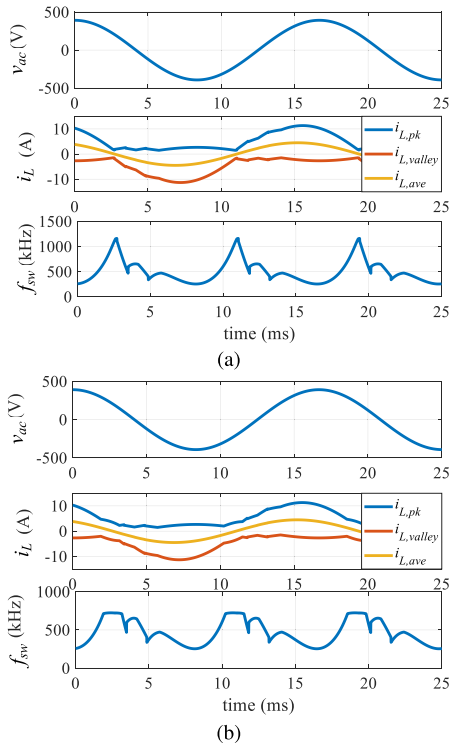

Fig. 9. Analytical waveforms of the CRM T-type totem-pole PFC rectifier at 0.79 leading PF when $V_{\text{in}} = 277\,\text{V}_{\text{ac}}, V_o = 480\,\text{V}_{\text{dc}}, L_b = 21\,\mu\text{H}, V_{\text{boun}} = 100\,\text{V}, P = 750\,\text{W}$, and $Q = -600\,\text{kVAr}$. (a) Peak frequency has no limitation. (b) Peak frequency is limited at 800 kHz.

limitation. Compared to Fig. 9(a), the peak switching frequency is limited to 800 kHz. The only drawback is that the inductor current ripple becomes larger during the ac current zero-crossing region with peak frequency limitation, which results in higher root mean square (RMS) current for higher loss and degrades the loss reduction benefit of frequency limitation. However, since the current ripple increment only occurs at low current during a short time within one line cycle, the rectifier power loss is still lower compared to the case without frequency limitation.

IV. Control Implementation

The proposed control strategy for the T-type totem-pole rectifier is shown in Fig. 10. To control the active power P and reactive power Q separately, instantaneous P and Q are estimated. The single-phase input current and voltage are sensed and converted into $\alpha\beta$ frame through a second-order generalized integrator-based orthogonal signal generator (OSG). Then, $\overrightarrow{v_{\alpha\beta}}$ and $\overrightarrow{i_{\alpha\beta}}$ are converted into dq rotating frame through Park transformation. Based on $\overrightarrow{v_{dq}}$ and $\overrightarrow{i_{dq}}$, the average active power P and reactive power Q are

$$P = \frac{1}{2}(v_d i_d + v_q i_q) \tag{10}$$

$$Q = \frac{1}{2}(v_q i_d - v_d i_q). \tag{11}$$

The input voltage magnitude V_m and phase angle θ are detected in a phase-locked loop (PLL), and a conditioned input voltage signal $v_{\text{ac,PLL}} = V_m \cos\theta$ is generated for the following control actions. The output voltage loop with a proportional

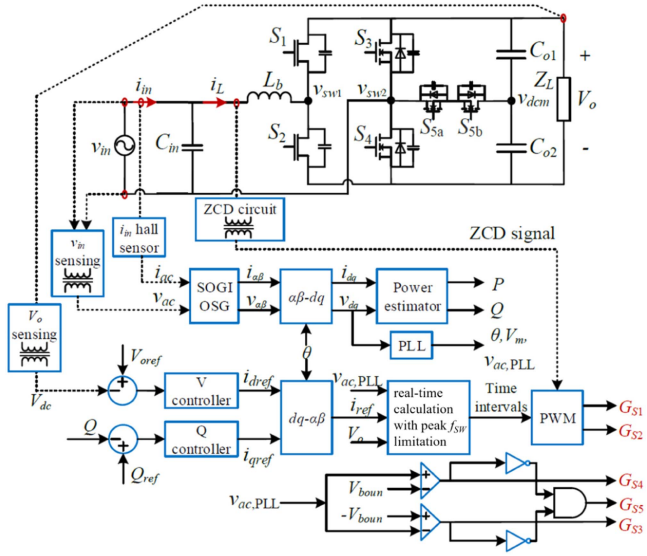

Fig. 10. Proposed control strategy of the T-type totem-pole rectifier.

integral (PI) compensator in d-axis regulates the output voltage and active power and produces the d-axis current reference $i_{d\text{ref}}$. In the q-axis, the conditioned reactive power Q is used to form a reactive power loop. Q is adjusted to follow the power reference Q_{ref} by a PI compensator, which generates the q-axis current reference $i_{q\text{ref}}$. In order to obtain the single-phase current reference i_{ref}, $i_{d\text{ref}}$ and $i_{q\text{ref}}$ are converted back to $\alpha\beta$ frame via the inverse Park transform. Then, the current reference together with the conditioned input and output voltages are transmitted to the real-time calculation where instantaneous switching time intervals are calculated based on the analytical model for full-range ZVS with reactive power operation. Gate signals of the GaN devices S_1 and S_2 are synchronized by the sensed inductor zero-current detection signal.

On the other hand, line-cycle switched Si MOSFETs are controlled according to the conditioned input voltage $v_{\text{ac,PLL}}$. With a defined boundary voltage V_{boun}, S_5 is turned ON to conduct the T-type mode when $|V_{\text{ac,PLL}}| \le V_{\text{boun}}$. Otherwise, totem-pole mode is adopted, where S_3 conducts during the negative half cycle when $v_{\text{ac,PLL}} < -V_{\text{boun}}$, and S_4 conducts during the positive half cycle when $v_{\text{ac,PLL}} > V_{\text{boun}}$.

The control implementation is simple and straightforward with hardware sensing circuits and one digital signal processing (DSP) microcontroller. The embedded real-time calculation does not require high processing capacity with the simplified and accurate modeling method proposed in [22]. Stable control is ensured by hardware sensing circuits that are designed with good noise immunity [25], [40].

V. Experimental Verification

To verify the design, a single-phase GaN-based CRM T-type totem-pole rectifier prototype is built and tested. Fig. 11 shows the physical prototype, and Table IV givea the detailed converter specifications. The rectifier main circuit is enclosed in a $90 \times 200 \times 43\,\text{mm}$ space, which is composed of the input EMI filter, boost inductor, GaN and Si devices, gate drive circuits, sensing

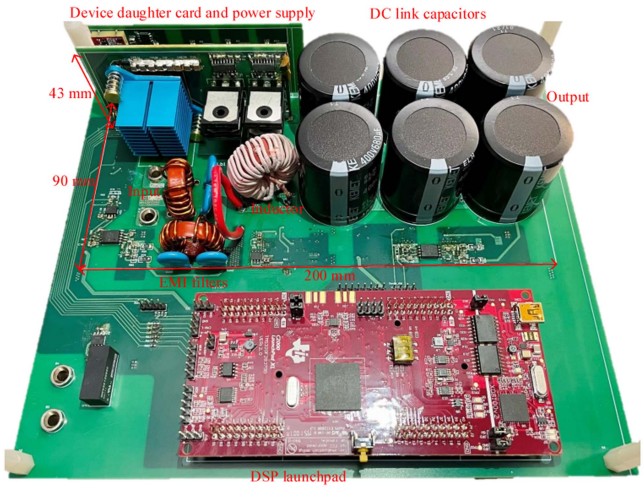

Fig. 11. Proposed control strategy of the T-type totem-pole rectifier.

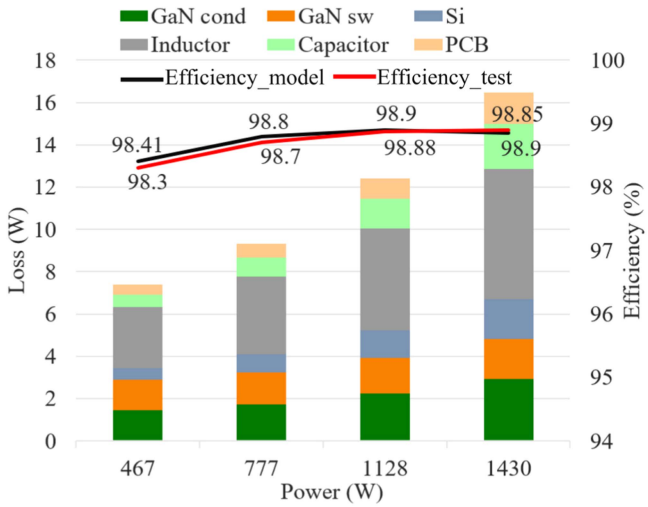

Fig. 12. Rectifier efficiency and power loss at different loading in unity PF.

TABLE IV
SPECIFICATIONS OF THE GAN-BASED RECTIFIER PROTOTYPE

Parameter	Value
Input voltage v_{in}	277 V_{ac}, 60 Hz
Output voltage V_o	480 V_{dc}
Active power rating P_o	1.5 kW
Apparent power rating S	1.6 kVA
Switching frequency f_{sw}	170–800 kHz
GaN devices S_1, S_2	GS66516 T, 650 V, 60 A
Si devices S_3, S_4, S_5	IPW65R019C7, 650 V
Boost inductor	21 μH, core Mix-2-T106
DC-link capacitor	900 μF, ELH687M400AT4AA
ZVS margin	$k_0 = 1.1$, $T_{\text{ZVS,min}} = 50$ ns
Two-stage EMI filter	$L_{CM1} = L_{CM2} = 438\ \mu$H $C_{CM1} = C_{CM2} = 10$ nF $L_{DM1} = L_{DM2} = 13\ \mu$H $C_{DM1} = C_{DM2} = 3\ \mu$F

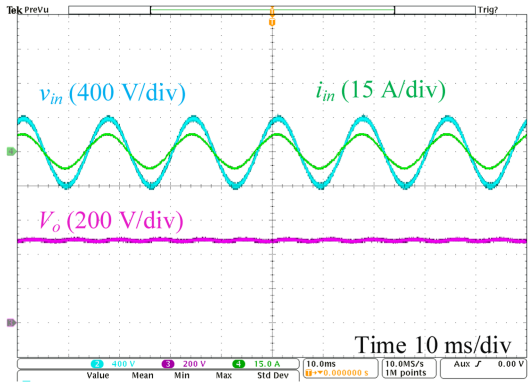

(a)

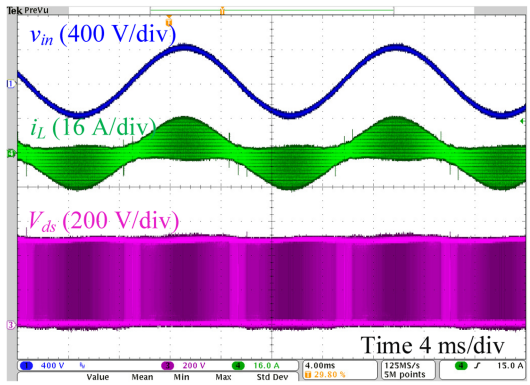

(b)

Fig. 13. Full-load experimental waveforms of the GaN-based CRM T-type totem-pole rectifier at unity PF when $v_{\text{in}} = 277\ V_{\text{ac}}$ and $V_o = 480\ V_{\text{dc}}$. (a) Waveforms of v_{in}, i_{in}, V_o. (b) Waveforms of v_{in}, i_{L}, V_{ds}.

circuits, auxiliary power supply, and the dc-link capacitors. A TMS320F28379D DSP launchpad from Texas Instruments is used as the controller.

A. Steady-State Operation

The prototype is first tested at steady-state operation. Fig. 12 shows the measured efficiency η at different loading in unity PF, and the full-load efficiency is 98.9% at unity PF. The rectifier efficiency and loss breakdown at each loading are also calculated based on the converter loss model [40], and the testing results match well with the prediction (see Fig. 12).

Figs. 13 and 14 show the detailed experimental waveforms of the GaN-based CRM T-type totem-pole rectifier prototype at full load at unity PF. The line cycle waveforms and switching cycle waveforms are presented. The input current is well-regulated in phase with the input voltage, and the output voltage is converted stably to $480\,V_{\text{dc}}$. The inductor current is regulated in CRM, and full-range ZVS operation is achieved in both the totem-pole mode and T-type mode.

Steady-state operation with different PFs is also demonstrated on the prototype. Fig. 15 shows the experimental waveforms of

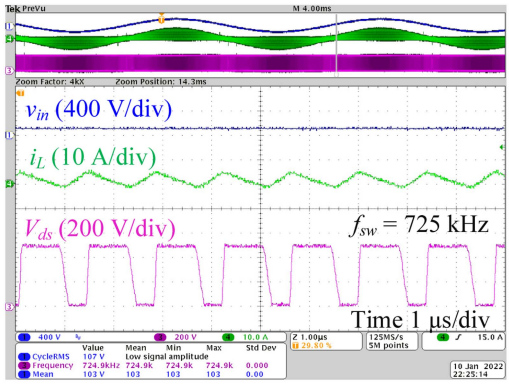

(a)

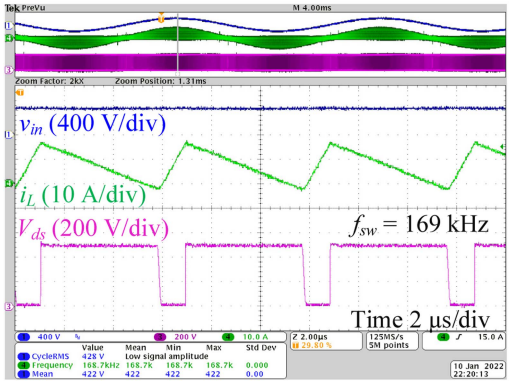

(b)

Fig. 14. Full-load switching waveforms of the GaN-based CRM T-type totem-pole rectifier at unity PF when $v_{\rm in} = 277\,{\rm V_{ac}}$ and $V_o = 480\,{\rm V_{dc}}$. (a) Waveforms of $v_{\rm in}$, $i_{\rm L}$, $V_{\rm ds}$ at during T-type mode. (b) Waveforms of $v_{\rm in}$, $i_{\rm L}$, $V_{\rm ds}$ during totem-pole mode.

TABLE V
OPERATION PERFORMANCE OF THE RECTIFIER PROTOTYPE AT FULL LOAD

	P (W)	Q (VAr)	PF	η	iTHD
Unity	1430	−166	> 0.99	98.9%	3.2%
Leading	1437	−499	0.94	98.8%	2.3%
Lagging	1435	516	0.94	98.6%	4.7%

TABLE VI
OPERATION PERFORMANCE OF THE RECTIFIER PROTOTYPE AT HALF LOAD

	P (W)	Q (VAr)	PF	η	iTHD
Unity	777	−93	> 0.99	98.7%	4.9%
Leading	782	−600	0.79	98.6%	3%
Lagging	779	431	0.87	98.54%	4.9%

the GaN-based T-type totem-pole rectifier at full load with 0.94 lagging PF [see Fig. 15(a)], at half load with 0.79 leading PF [see Fig. 15(b)], and at half load with 0.87 lagging PF [see Fig. 15(c)]. Tables V and VI give the measured operation performance at full and half loads, respectively. In each operation, the reactive power and phase shift between $v_{\rm in}$ and $i_{\rm in}$ are regulated accurately. The

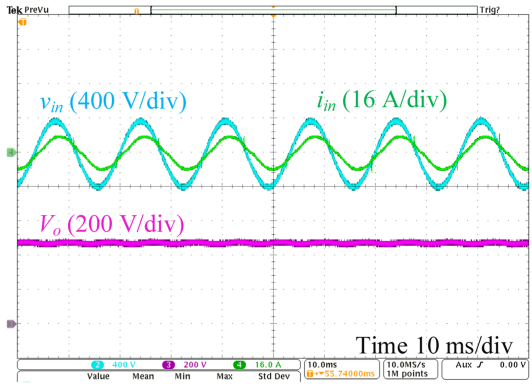

(a)

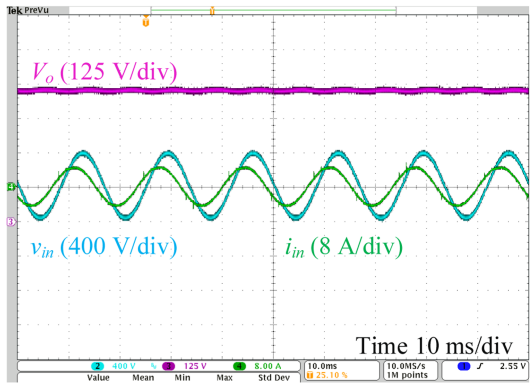

(b)

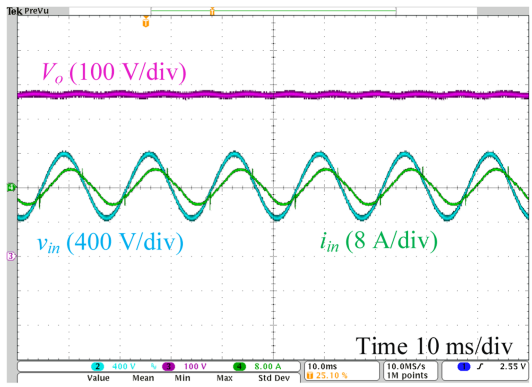

(c)

Fig. 15. Experimental waveforms of the GaN-based CRM T-type totem-pole rectifier prototype at (a) 0.94 lagging PF with $P = 1435\,{\rm W}$ and $Q = 516\,{\rm VAr}$; (b) 0.79 leading PF with $P = 782\,{\rm W}$ and $Q = -600\,{\rm VAr}$; and (c) 0.87 lagging PF with $P = 779\,{\rm W}$ and $Q = -431\,{\rm VAr}$ when $v_{\rm in} = 277\,{\rm V_{ac}}$ and $V_o = 480\,{\rm V_{dc}}$.

tested efficiency at full and half loads is above 98.5% and the input current THD is below 5%.

One issue that can be observed in Figs. 13–15 is the current spike during the mode transition between the totem-pole mode and T-type mode. This is because of the implementation limitation of DSP for PWM generation. Ideally, once the mode transition is detected, hardware Si MOSFETs (S_3–S_5) switching and the GaN device PWM updating should be conducted simultaneously to enable modulation change. However, since the CRM rectifier has a wide switching frequency range, the

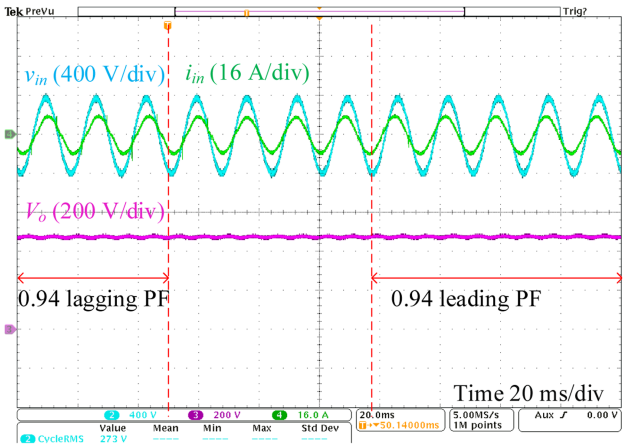

Fig. 16. Experimental waveform of the rectifier prototype from 0.94 lagging PF to 0.94 leading PF at full load when $v_{\text{in}} = 277\,\text{V}_{\text{ac}}$ and $V_o = 480\,\text{V}_{\text{dc}}$.

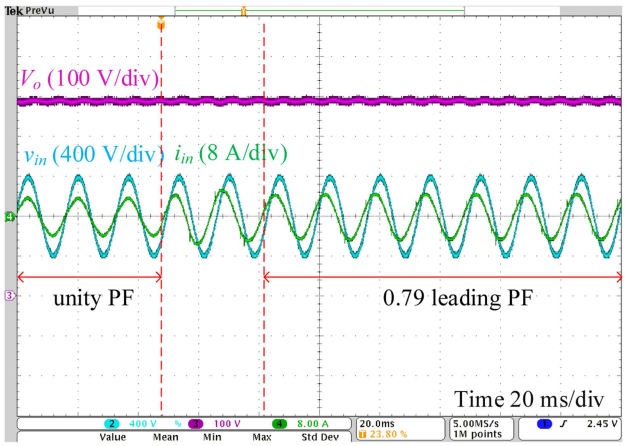

Fig. 17. Experimental waveform of the rectifier prototype from unity PF to 0.79 leading PF at half load when $v_{\text{in}} = 277\,\text{V}_{\text{ac}}$ and $V_o = 480\,\text{V}_{\text{dc}}$.

PWM updating at each switching frequency cannot be synchronized instantaneously with the real-time calculation and Si MOSFETs' switching in the DSP. Therefore, the inductor voltage may change suddenly while PWM is not updated, and current spike occurs due to the unbalanced inductor volt-second in a few switching cycles. Although such current spike degrades the ac current, the tested current THD still meets the typical standard [24].

B. Dynamic Operation

The rectifier prototype is also demonstrated during dynamic operation among different PFs. Fig. 16 shows the experimental waveforms at full load when the rectifier transitions from 0.94 lagging PF to 0.94 leading PF. The reactive power reference Q_{ref} linearly changes within four line cycles, and the phase shift between v_{in} and i_{in} is adjusted gradually without current overshoot. Fig. 17 shows the experimental waveforms at half load when the rectifier transitions from unity PF to 0.79 leading PF. With a step change in Q_{ref}, the dynamic response lasts for two line cycles, which is limited by the reactive power loop bandwidth at 30 Hz. Faster dynamic response can be achieved by designing the reactive power control loop with higher bandwidth. Still, the rectifier performs a smooth dynamic response without current overshoot, and the output voltage regulation is not disturbed. Therefore, flexible reactive power regulation with smooth dynamic response is validated in the GaN-based CRM T-type totem-pole rectifier.

VI. Conclusion and Discussions

This article proposed a single-phase GaN-based rectifier with ZVS operation and reactive power transfer capability. The GaN-based CRM totem-pole PFC rectifier is able to achieve high efficiency with ZVS control, but has control challenge during the ac voltage zero-crossing when extending to nonunity PF operation. To overcome the ac voltage zero-crossing challenge, a T-type totem-pole rectifier was proposed where a bidirectional switch was added to modify the converter's modulation during the voltage zero-crossing region. A full-range ZVS modulation with peak frequency limitation was proposed to realize GaN devices' ZVS turn-ON at both unity PF operation and nonunity PF operation. Also, a digital-based control strategy with separate power control loops and model-based real-time calculation was developed.

The proposed topology, ZVS modulation, and control scheme were verified experimentally on a 1.6-kVA GaN-based rectifier prototype. Full-range ZVS turn-ON of GaN devices was achieved, and the measured full-load efficiency of the rectifier at unity PF was 98.9%. Reactive power transfer capability of the rectifier prototype was validated at 0.94, 0.87, and 0.79 PF, and the tested efficiency was above 98.5%. The rectifier prototype was also demonstrated during dynamic transition among different PFs, and flexible reactive power regulation with smooth dynamic response was achieved.

With the bidirectional rectifier topology and separate controls of active power and reactive power, the rectifier can also work at lower PFs with more reactive power. The capacity of reactive power transfer depends on the rectifier's specifications, including the power rating and physical components design, such as inductor, capacitor, and devices. Also, since the input ac voltage is conditioned through an OSG-based PLL, the control method will not be impacted by ac voltage variations or distortions as long as the ac voltage phase information is correct from the PLL.

The proposed single-phase GaN-based T-type totem-pole rectifier is a promising candidate for front-end rectifier in applications, such as data center and telecommunication power supply. At the power system level, the rectifiers cannot only provide stable dc power for critical loads, but also participate in grid support to provide fast and flexible reactive power compensation. Advantageous in small size and high efficiency, the proposed rectifier can be used as an efficient alternative to centralized bulky power compensators for managing the power system. Considerations in intelligent monitoring and efficient assignment of reactive power demand to distributed rectifiers are required. For complicated system, such as data centers, a supervisory central controller is required to achieve grid reactive power support.

REFERENCES

[1] S. R. Islam, S. Maxwell, M. K. Hossain, S.-Y. Park, and S. Park, "Reactive power distribution strategy using power factor correction converters for smart home application," in *Proc. IEEE Energy Convers. Congr. Expo.*, 2016, pp. 1–6.

[2] C. Nie, Y. Wang, W. Lei, M. Chen, and Y. Zhang, "An enhanced control strategy for multiparalleled grid-connected single-phase converters with load harmonic current compensation capability," *IEEE Trans. Ind. Electron.*, vol. 65, no. 7, pp. 5623–5633, Jul. 2018.

[3] D. Xiao, M. Chen, and Y. Chen, "Negative sequence current and reactive power comprehensive compensation for freight railway considering the impact of DFIGs," *CPSS Trans. Power Electron. Appl.*, vol. 6, no. 3, pp. 235–241, Sep. 2021.

[4] J. Dixon, L. Moran, J. Rodriguez, and R. Domke, "Reactive power compensation technologies: State-of-the-art review," *Proc. IEEE*, vol. 93, no. 12, pp. 2144–2164, Dec. 2005.

[5] S. K. Mondal, "Active and reactive power compensation of data center using multi-level STATCOM inverter," in *Proc. IEEE Int. Symp. Power Electron. Distrib. Gener. Syst.*, 2016, pp. 1–8.

[6] ABB, "PCS100 STATCOM-dynamic reactive power compensation, technical catalogue," 2014, Accessed: Dec. 2020. [Online]. Available: https://library.e.abb.com/

[7] J. Kueck, B. Kirby, T. Rizy, F. Li, and N. Fall, "Reactive power from distributed energy," *Electricity J.*, vol. 19, no. 10, pp. 27–38, 2006.

[8] M. Singh, V. Khadkikar, A. Chandra, and R. K. Varma, "Grid interconnection of renewable energy sources at the distribution level with power-quality improvement features," *IEEE Trans. Power Del.*, vol. 26, no. 1, pp. 307–315, Jan. 2011.

[9] D. Boroyevich, I. Cvetkovic, R. Burgos, and D. Dong, "Intergrid: A future electronic energy network?," *IEEE Trans. Emerg. Sel. Topics Power Electron.*, vol. 1, no. 3, pp. 127–138, Sep. 2013.

[10] H. Cheng, T. Chen, C. Wang, Z. Zhao, Z. Li, and Y. Guan, "Single-phase bridgeless rectifier based system with enhanced capability of reactive power compensation," *IEEE Access*, vol. 7, pp. 181444–181457, 2019.

[11] Z. Tang, D. J. Hill, and T. Liu, "Fast distributed reactive power control for voltage regulation in distribution networks," *IEEE Trans. Power Syst.*, vol. 34, no. 1, pp. 802–805, Jan. 2019.

[12] U.S. Department of Energy, "Load participation in ancillary services workshop report," 2011, Accessed: Dec. 2020. [Online]. Available: https://www.energy.gov/eere/analysis/downloads

[13] S. M. Kaviri, M. Pahlevani, B. Mohammadpour, P. Jain, and A. Bakhshai, "Power control of a bi-directional AC/DC rectifier used for telecom backup systems," in *Proc. IEEE Int. Telecommun. Energy Conf.*, 2015, pp. 1–5.

[14] N. Akel, M. Pahlevaninezhad, and P. Jain, "A D-Q rotating frame reactive power controller for single-phase bidirectional converters," in *Proc. IEEE 36th Int. Telecommun. Energy Conf.*, 2014, pp. 1–5.

[15] L. Liu, H. Li, Y. Xue, and W. Liu, "Reactive power compensation and optimization strategy for grid-interactive cascaded photovoltaic systems," *IEEE Trans. Power Electron.*, vol. 30, no. 1, pp. 188–202, Jan. 2015.

[16] R. Kabiri, D. G. Holmes, B. P. McGrath, and L. G. Meegahapola, "LV grid voltage regulation using transformer electronic tap changing, with PV inverter reactive power injection," *IEEE Trans. Emerg. Sel. Topics Power Electron.*, vol. 3, no. 4, pp. 1182–1192, Dec. 2015.

[17] M. A. Fasugba and P. T. Krein, "Gaining vehicle-to-grid benefits with unidirectional electric and plug-in hybrid vehicle chargers," in *Proc. IEEE Veh. Power Propulsion Conf.*, 2011, pp. 1–6.

[18] S. M. Park and S.-Y. Park, "Versatile control of unidirectional AC–DC boost converters for power quality mitigation," *IEEE Trans. Power Electron.*, vol. 30, no. 9, pp. 4738–4749, Sep. 2015.

[19] M. C. Kisacikoglu, M. Kesler, and L. M. Tolbert, "Single-phase on-board bidirectional PEV charger for V2G reactive power operation," *IEEE Trans. Smart Grid*, vol. 6, no. 2, pp. 767–775, Mar. 2015.

[20] W. Song, Z. Deng, S. Wang, and X. Feng, "A simple model predictive power control strategy for single-phase PWM converters with modulation function optimization," *IEEE Trans. Power Electron.*, vol. 31, no. 7, pp. 5279–5289, Jul. 2016.

[21] A. Q. Huang, "Wide bandgap (WBG) power devices and their impacts on power delivery systems," in *Proc. IEEE Int. Electron Devices Meeting*, 2016, pp. 20.1.1–20.1.4.

[22] J. Sun, X. Huang, N. N. Strain, D. J. Costinett, and L. M. Tolbert, "Inductor design and ZVS control for a GaN-based high efficiency CRM totem-pole PFC converter," in *Proc. IEEE Appl. Power Electron. Conf. Expo.*, 2019, pp. 727–733.

[23] Z. Huang, Z. Liu, F. C. Lee, and Q. Li, "Critical-mode-based soft-switching modulation for high-frequency three-phase bidirectional AC–DC converters," *IEEE Trans. Power Electron.*, vol. 34, no. 4, pp. 3888–3898, Apr. 2019.

[24] Z. Liu, F. C. Lee, Q. Li, and Y. Yang, "Design of GaN-based MHz totem-pole PFC rectifier," *IEEE Trans. Emerg. Sel. Topics Power Electron.*, vol. 4, no. 3, pp. 799–807, Sep. 2016.

[25] J. Sun et al., "Mitigation of current distortion for GaN-based CRM totem-pole PFC rectifier with ZVS control," *IEEE Open J. Power Electron.*, vol. 2, pp. 290–303, 2021.

[26] Q. Huang, R. Yu, Q. Ma, and A. Q. Huang, "Predictive ZVS control with improved ZVS time margin and limited variable frequency range for a 99% efficient, 130-W/in^3 MHz GaN totem-pole PFC rectifier," *IEEE Trans. Power Electron.*, vol. 34, no. 7, pp. 7079–7091, Jul. 2019.

[27] Q. Huang and A. Q. Huang, "Review of GaN totem-pole bridgeless PFC," *CPSS Trans. Power Electron. Appl.*, vol. 2, no. 3, pp. 187–196, Sep. 2017.

[28] J. Li, R. Qin, J. Sun, and D. Costinett, "Systematic design of a 100-W 6.78-MHz wireless charging station covering multiple devices and a large charging area," *IEEE Trans. Power Electron.*, vol. 37, no. 4, pp. 4877–4889, Apr. 2022.

[29] Y. Tang, W. Ding, and A. Khaligh, "A bridgeless totem-pole interleaved PFC converter for plug-in electric vehicles," in *Proc. IEEE Appl. Power Electron. Conf. Expo.*, 2016, pp. 440–445.

[30] T. T. Vu and E. Mickus, "99% efficiency 3-level bridgeless totem-pole PFC implementation with low-voltage silicon at low cost," in *Proc. IEEE Appl. Power Electron. Conf. Expo.*, 2019, pp. 2077–2083.

[31] Q. Huang, Q. Ma, P. Liu, A. Q. Huang, and M. de Rooij, "3kW four-level flying capacitor totem-pole bridgeless PFC rectifier with 200V GAN devices," in *Proc. IEEE Energy Convers. Congr. Expo.*, 2019, pp. 81–88.

[32] Z. Liu, "Characterization and application of wide-band-gap devices for high frequency power conversion," Ph.D. dissertation, Virginia Tech, Blacksburg, VA, USA, 2017.

[33] J. Sun, J. Li, D. J. Costinett, and L. M. Tolbert, "A GaN-based CRM totem-pole PFC converter with fast dynamic response and noise immunity for a multi-receiver WPT system," in *Proc. IEEE Energy Convers. Congr. Expo.*, 2020, pp. 2555–2562.

[34] Y. Yang, Z. Liu, F. C. Lee, and Q. Li, "Multi-phase coupled and integrated inductors for critical conduction mode totem-pole PFC converter," in *Proc. IEEE Appl. Power Electron. Conf. Expo.*, 2017, pp. 1804–1809.

[35] B. Sun, "Control challenges in a totem-pole PFC," *Analog Appl. J.*, vol. 2, pp. 1–4, 2017.

[36] L. Xue, Z. Shen, D. Boroyevich, and P. Mattavelli, "GaN-based high frequency totem-pole bridgeless PFC design with digital implementation," in *Proc. IEEE Appl. Power Electron. Conf. Expo.*, 2015, pp. 759–766.

[37] R. A. Siddique, R. Khandekar, P. Ksiazek, and J. Wang, "Investigation of zero-crossing common-mode noise and current spike in GaN based totem-pole PFC," in *Proc. IEEE Can. Conf. Elect. Comput. Eng.*, 2018, pp. 1–5.

[38] B. Sun, "How to reduce current spikes at AC zero-crossing for totem-pole PFC," *Analog Appl. J.*, pp. 23–26, 2015.

[39] B. Zhang, Q. Lin, J. Imaoka, M. Shoyama, S. Tomioka, and E. Takegami, "EMI prediction and reduction of zero-crossing noise in totem-pole bridgeless PFC converters," *J. Power Electron.*, vol. 19, no. 1, pp. 278–287, 2019.

[40] J. Sun, "Data center power system emulation and GaN-based high-efficiency rectifier with reactive power regulation," *Ph.D. dissertation*, Univ. Tennessee, Knoxville TN, USA, 2022.